Neoplasia • Vol. 7, No. 4, April 2005, pp. 369–379 369

www.neoplasia.com

[18F]FDG Uptake and PCNA, Glut-1, and Hexokinase-II Expressions in Cancers and Inflammatory Lesions of the Lung

Marcelo Mamede, Tatsuya Higashi*, Masanori Kitaichi†, Koichi Ishizu*, Takayoshi Ishimori*, Yuji Nakamoto*, Kazuhiro Yanagihara‡, Mio Li‡, Fumihiro Tanaka‡, Hiromi Wada‡, Toshiaki Manabe† and Tsuneo Saga**

*Department of Nuclear Medicine and Diagnostic Imaging, †Pathology and ‡Thoracic Surgery, Graduate School of Medicine, Kyoto University, Kyoto, Japan

Abstract

***PURPOSE*: The aim of this study was to evaluate the relationships among [18F]fluorodeoxyglucose ([18F]-FDG) uptake, Glut-1 and HK-II expressions, and grade of inflammation in resected lung lesions. *MATERIALS AND METHODS*: Sixty patients had undergone preoperative 18F-FDG-PET imaging and thoracotomy. For semiquantitative analysis of 18F-FDG uptake, partial volume effect corrected maximum standardized uptake values (pSUVs) were calculated. Immunohistochemical staining was performed in resected specimens using anti–Glut-1, anti–HK-II, and anti–proliferative cellular nuclear antigen (PCNA) antibodies, and immunoreactivities were scored as G-, H-, and P-indexes on a five-point scale (0: 0%; 1: ~20%, 2: ~40%; 3: ~60%; 4: ~80%, and 5: ~100% percentages of strongly immunoreactive cells). Grade of inflammation was also evaluated. *RESULTS*: The malignant lesions had higher pSUV and higher G- and H-indexes than nonmalignant lesions. pSUVs correlated with the G- ($p < .001$), H- ($p < .01$), and P-indexes ($p < 0.01$) in malignant lesions. In adenocarcinomas, cancers with lower differentiation showed higher expression of Glut-1 and HK-II than those with higher differentiation. A positive linear regression was observed between pSUVs and the grading of inflammation in nonmalignant lesions ($p < 0.05$). *CONCLUSIONS*: Our study indicates that 18F-FDG uptake in lung cancer correlates well with Glut-1, HK-II, and PCNA expression. For nonmalignant lesions, the presence of a higher inflammatory process correlated with 18F-FDG uptake.**

Neoplasia (2005) **7,** 369–379

Keywords: PCNA, HK-II, Glut-1, [18F]FDG-PET, lung cancer.

Introduction

Lung cancer is the most common cause of cancer death in the United States and Japan [1,2]. In Japan, lung cancer was responsible for 22.0% of deaths in men and 12.7% in women, being characterized as the first and second most common cause of death, respectively [2].

It has long been recognized that cancer cells have increased rates of glucose metabolism compared to healthy cells [3,4]. A variety of mechanisms have been proposed for the accelerated glucose use seen in growing tumors and in transformed and malignant cells [5]. Transmembrane transport mediated by specific transporters [6] is considered to be one of the most important mechanisms for enhancing glucose influx into cells. Furthermore, increased concentrations of hexokinase [7,8] with decreased rates of glucose-6-phosphatase [9] have been reported to accelerate glucose phosphorylation, which results in increased glucose consumption. Among several subtypes, glucose transporter protein, type 1 (Glut-1) and glucose phosphorylation enzyme type II (Hexokinase II, or HK-II) are known to be the most important subtypes for glucose metabolism in cancer cells [10–14].

Positron emission tomography (PET) imaging with [18F]fluorodeoxyglucose ([18F]FDG) has become an important nonlinvasive technique for the evaluation of solitary pulmonary nodules, cancer staging, detection of recurrent neoplasms, and radiotherapy planning [15–21]. The rationale for the use of [18F]FDG is based on the increase glucose metabolism of malignant cells, in which [18F]FDG, an analogue of glucose, is absorbed, phosphorylated, and trapped in the cytosol of the cells. However, the exact mechanism of [18F]FDG accumulation in malignant lesions has not been fully elucidated.

In addition, [18F]FDG uptake is not specific for malignancy; some benign abnormalities can demonstrate increased tracer activity as well [22]. Some studies showed low specificity of the diagnostic value of [18F]FDG-PET in differentiation between

Abbreviations: Glut-1, glucose transporter protein, type 1; HK-II, glucose phosphorylation enzyme type II, Hexokinase II; PCNA, proliferative cellular nuclear antigen; SUV, maximum standardized uptake value; pSUV, partial volume effect corrected maximum standardized uptake value; BG SUV, background SUV; ROI, region of interest

Address all correspondence to: Tatsuya Higashi, MD, PhD, Department of Nuclear Medicine and Diagnostic Imaging, Graduate School of Medicine, Kyoto University, Sakyo, Kyoto 606-8507, Japan. E-mail: higashi@kuhp.kyoto-u.ac.jp

Received 25 August 2004; Revised 7 November 2004; Accepted 8 November 2004.

DOI 10.1593/neo.04577

cancer and benign diseases. These studies have addressed the problem of differentiation between malignant lesions and granulomatous infections, including pulmonary tuberculosis (TB) and histoplasmosis [22–25].

In the present study, we examined the immunohistochemical expressions of Glut-1, HK-II, and the proliferative marker (proliferative cellular nuclear antigen, or PCNA) in pulmonary lesions (malignant and nonmalignant) to elucidate the mechanism of [^{18}F]FDG accumulation. We also evaluated potential differences in the expression pattern of these three antigens among various histologic types and compared the results with clinical data.

Materials and Methods

Subjects of the Study

In this prospective study, 60 patients (38 men, 22 women; age range, 26–79 years old; mean age, 65.0 ± 11.5 years old) with 41 primary lung cancers, 5 pulmonary metastatic lesions, and 14 nonmalignant lesions who had undergone both preoperative [^{18}F]FDG-PET imaging and thoracotomy were enrolled in this study. All patients underwent thoracotomy within 4 weeks after their [^{18}F]FDG-PET study. Final diagnoses and sizes of the primary tumors were confirmed histopathologically in resected specimens obtained by thoracotomy in all patients. None of them received any previous chemotherapeutic or radiotherapeutic treatments. None of the patients had diabetes, and the serum glucose level just before [^{18}F]FDG injection was less than 120 mg/dl in all patients. Before being enrolled in this study, each patient gave written informed consent, as required by the Kyoto University Human Study Committee.

PET Study

^{18}F was produced by a ^{20}Ne (d, alpha) ^{18}F nuclear reaction, and [^{18}F]FDG was synthesized by the nucleophilic substitution method using an [^{18}F]FDG-synthesizing instrument F-100 (Sumitomo Heavy Industries, Co. Ltd., Tokyo, Japan) and a cyclotron, CYPRIS-325R (Sumitomo Heavy Industries, Co. Ltd.) [26,27]. All patients were examined with a high-resolution, whole-body PET scanner with an 18-ring detector arrangement (Advance; General Electric Medical systems, Milwaukee, WI).

The patients fasted for more than 4 hours before the injection of [^{18}F]FDG. All subjects received an intravenous injection of [^{18}F]FDG (296 ± 74 MBq), and the acquisition of whole-body PET images started 50 minutes later. The patient laid supine on the PET table with the arms positioned on the sides. The patient was then fixed in place by wrapping a holding belt around the abdomen. Data acquisition (emission and transmission scan) was performed in two-dimensional imaging mode with septae in place. Emission images were acquired for 3 minutes per bed position, and each postemission transmission scan was obtained for 1 minute per position. Whole-body scan (from face to upper thigh) was performed in each patient using five or six bed positions according to the height of each patient. The data were reconstructed using the ordered subsets expectation maximization method (OSEM) using 16 subsets, 3 iterations, and 128 × 128 array size.

Image Analysis

PET images were interpreted by at least three experienced nuclear medicine physicians with all available clinical information and correlative conventional imaging as anatomic guidance. For semiquantitative analysis of the [^{18}F]FDG uptake, regions of interest (ROI) were manually defined on transaxial tomograms. ROI were placed on the lesions using a semiautomated method that encompassed all pixels that had uptake values of greater than 90% of the maximum uptake in that slice. In patients for whom no nodules were detectable by PET, the ROI was drawn based on the chest CT scans. The maximum standardized uptake value (SUV) was used for the quantitative analysis of tumor [^{18}F]FDG uptake:

$$\mathrm{SUV} = \frac{C\ (\mathrm{kBq/ml})}{\mathrm{ID}\ (\mathrm{kBq})/\mathrm{body\ weight}\ (\mathrm{kg})} \quad (1)$$

where C represents tissue activity concentration measured by PET, and ID represents the injected dose. By using the average diameter of the resected tumor, the SUV data were corrected for partial volume effects (PVE) in lesions with diameter <2.8 cm, based on recovery coefficient (RC) curve. RC was calculated in our institution using spherical phantoms based on the method of Akashi et al. [28] (data not shown). Each RC based on the RC curve was applied to the correction of SUV using background activity (BG SUV) as previously described [29]:

$$\underset{(\mathrm{pSUV})}{\mathrm{PVE\ corrected\ SUV}} = \mathrm{BG\ SUV} + \frac{(\mathrm{measured\ SUV} - \mathrm{BG\ SUV})}{\mathrm{RC}} \quad (2)$$

BG SUV was defined as average SUV on a 10 × 10-pixel ROI adjacent to the tumor. This ROI was placed either medial or lateral to the tumor to minimize anteroposterior background variations, and away from the chest wall and mediastinum [30]. A lesion with SUV or partial volume effect corrected maximum standardized uptake value (pSUV) higher than 2.5 was considered positive for malignancy.

Histologic Examination

All the patients underwent surgical resection of the lung nodule. Paraffin-embedded specimens were processed for anti–Glut-1, anti–HK-II, or anti–PCNA immunostaining or routine hematoxylin–eosin staining. The polyclonal rabbit anti–glucose transporter antibody reactive with human Glut-1 (brain/erythrocyte type) and the monoclonal mouse antiproliferating cell nuclear antigen (PCNA) antibody reactive with proliferating human cells were purchased from DAKO (Carpinteria, CA). Both antibodies were diluted

1:200 with 0.05 mol/l Tris–HCl buffer containing a carrier protein and 0.015 mol/l sodium azide. The polyclonal rabbit anti-hexokinase antibody reactive with rat HK-II isoenzyme was purchased from Chemicon International, Inc. (Temecula, CA). It was diluted 1:500 with 0.05 mol/l Tris–HCl buffer containing a carrier protein and 0.015 mol/l sodium azide.

Paraffin was removed from sections of each tumor using xylene (3 × 5 minutes) and ethanol in various dilutions. Before immunohistochemical procedures, unmasking treatments were performed on all sections, following previous established procedure [30]. Sections for anti–Glut-1 immunostaining were incubated with target retrieval solution (TRS; DAKO), using the hot bath methods at 95°C to 99°C for 20 minutes. The other sections, including those for anti–HK-II and anti-PCNA immunostaining, were unmasked by the microwave method using a distilled water bath for 15 minutes.

After 20 minutes of cooling, the sections were washed with phosphate-buffered saline (PBS), containing 20 mmol/l sodium phosphate and 150 mmol/l NaCl (pH 7.0), for 15 minutes. Then, the endogenous peroxidase activities were blocked for 10 minutes at room temperature (RT) with 0.3% hydrogen peroxide in distilled water, and were washed with PBS for 5 minutes. Nonspecific binding was blocked for 30 minutes at RT with a blocking buffer solution (DAKO), which contained 10% normal bovine serum in PBS. In the next step, each section was incubated with the anti-PCNA, anti–Glut-1, or anti–HK-II antibodies as a primary antibody for 1 hour at RT. Parallel sections were incubated with healthy rabbit IgG (20 μg/ml) as negative controls.

Then, all the sections were washed with PBS with 0.05% polyoxyethylene sorbitan monolaurate (Tween 20; Kanto Chemical Co., Tokyo, Japan) for 15 minutes. In the following steps, each section was stained by the horseradish peroxidase (HRP)–labeled polymer method, using an Envision Kit/HRP 3,3′-diaminobenzidine tetrahydrochloride (DAB; DAKO). For linking, the sections were incubated with the labeled polymer for 60 minutes at RT and washed with PBS with 0.05% Tween 20 for 15 minutes. As a substrate–chromogen solution, DAB was used at RT for 10 minutes, and diluted at 1 mg/ml with 0.05 mol/l Tris–HCl buffer, pH 7.5. All sections were then rinsed gently and washed with distilled water for 5 minutes. In the final step, the sections were lightly counterstained with Mayer's hematoxylin for 4 minutes, and then washed in a running water bath. The sections were then dehydrated twice by ethanol bath for 2 minutes and then dried. A coverslip was positioned with mounting media. All slides were examined by light microscopy.

Microscopic Analysis

Forty-one primary malignant lesions, 5 metastatic specimens, and 14 nonmalignant specimens were available for pathologic evaluation. A well-experienced pathologist in lung diseases (M.K.) reviewed all of the pathologic materials. In those cases of neoplastic lesions, tumor type [adenocarcinoma (AC), squamous cell carcinoma (SCC), etc.], tumor subtype (papillary, acinar, tubular, and mucinous), differentiation (poorly, moderately, or well differentiated), surgico-pathologic stage, and inflammatory changes were evaluated on each specimen. For those specimens of non-neoplastic lesions, the main diagnosis (e.g., tuberculosis, obstructive pneumonia), inflammatory changes, and/or fibrotic changes were carefully evaluated. In terms of inflammatory changes, a specific grading was performed on a four-point scale for all specimens (malignant and nonmalignant) based on the infiltrative inflammatory cells presented in the specimen as follows: 0—negative, 1—mild, 2—moderated, and 3—marked. This analysis was performed twice and averaged for further comparisons without significant variability.

Immunohistochemical analyses for anti–Glut-1 and anti–HK-II antibodies were independently performed twice by three well-experienced physicians who were unaware of the pSUVs. In each analysis, the percentages of strongly immunoreactive tumor cells in the total tumor cells was visually analyzed in several low-power fields (original magnification, 10 × 10) covering the entire specimen, and the average percentage was calculated and scored on a five-point scale (0: 0%; 1: 1–20%; 2: 21–40%; 3: 41–60%; 4: 61–80%; 5: 81–100%) for each counting trial. Then, scores from two counting trials were averaged again to give the Glut-1 expression index (*G*-index) or HK-II expression index (*H*-index).

To count PCNA-positive tumor cells, we followed the method described by Higashi et al. [32]. First, the sections were scanned in low-power fields to determine representative areas. High-power fields (× 20) were used for counting. Each analysis was performed in a minimum of 10 high-power fields with a total of two analyses per physician. All nuclei that showed a brown stain were considered to be positive. The proliferative fraction of tumor cells was counted by the percentage of PCNA-positive cells (PCNA-positive cells/total tumor cells). Furthermore, the average percentage was calculated and scored on a five-point scale in the same manner performed for Glut-1 and HK-II for each counting trial. Then all scores from two counting trials per each physician were averaged again to give the PCNA expression index (*P*-index).

As for nonmalignant lesions, immunohistochemical analyses for anti–Glut-1, anti–HK-II, and anti-PCNA antibodies were performed in the same manner described above. However, the percentage of strongly immunoreactive nontumor cells was compared to the total nontumor cells analyzed in several low-power fields (original magnification, 10 × 10) covering the entire specimen. The average percentage was calculated and scored on a five-point scale (as described above for malignant lesions).

Statistical Analysis

Data are expressed as mean ± standard deviation (SD). Simple comparisons using Student's *t* test were applied to compare two groups of different pathologies, whereas a multiple comparison (one-way ANOVA) was also applied between several groups of histologic diagnoses. Analyses

Table 1. Patient Characteristics (Malignant Lesions).

Diagnosis	Type	Size (mm)	SUV	pSUV
Primary (n = 41)				
Adenocarcinoma (n = 32)	Acinar (n = 5)	23.8 ± 8.3	6.3 ± 5.5	6.9 ± 5.5
	Acinar/pap (n = 1)	50.0	11.6	11.6
	Papillary (n = 23)	21.1± 9.1	5.8 ± 3.7	7.7 ± 4.2
	Solid growth (n = 2)	34.0 ± 15.6	17.8 ± 7.9	18.3 ± 7.3
	Tubular (n = 1)	20.0	23.8	29.5
	Total	23.2 ± 10.5	7.3 ± 5.8	9.0 ± 6.3
SCC (n = 6)	–	32.7 ± 16.0	15.2 ± 4.7	19.5 ± 7.5
Neuroendocrine	Epithelial	6	3.5	11.8
Thymoma	Large cell	78	6.6	6.6
Pleomorphic carc	Lymphocyte	50	23.3	23.3
Metastatic (n = 5)				
Adenocarcinoma	Acinar	17	12.4	19.0
SCC	–	25	16.4	16.1
Renal Ca	Clear cell	15	4.5	7.9
Esophageal Ca	–	10	2.3	6.5
PNET	Skin tumor	70	4.0	4.0
Total (n = 46)		26.3 ± 15.8	8.7 ± 6.4	10.9 ± 7.3

SUV = nonpartial volume effect corrected maxSUV; pSUV = partial volume effect corrected maxSUV; SCC = squamous cell carcinoma of the lung; pleomorphic carc = pleomorphic carcinoma; Ca = cancer; PNET = primary neuroendocrine tumor; acinar/pap = acinar and papillary type.

of correlation were carried out using a Spearman rank test, as well as linear regression analyses. All statistical analyses were performed using SPSS version 9.0. Values were considered significant at $P < .05$.

Results

Histologic Findings

Table 1 summarizes the characteristics of patients with malignant lesions in this study. Among the 41 primary pulmonary malignant lesions, 32 were diagnosed as AC (78.1%), six were diagnosed as SCC (14.6%), and the remaining three lesions (7.3%) were diagnosed as other primary lung tumors. Most of the patients (80.5%) had an early stage of disease (stages I and II). Five lesions were diagnosed as metastatic lesions. Maximal tumor diameters, estimated from histopathologic specimen, ranged from 0.6 to 7.8 cm. The SCCs showed larger diameters than ACs, but not statistically significant. No significant correlations were observed among size of nodules, stage of disease, and differentiation of the tumor.

Table 2 summarizes the characteristics of patients with nonmalignant lesions. Ten lesions (71.4%) were considered as TB. Maximal tumor diameters ranged from 1.0 to 4.3 cm. The sizes of nonmalignant lesions were relatively smaller than those observed for malignant lesions (NS).

[^{18}F]FDG PET Findings

Using a cutoff value of 2.5 for SUV, [^{18}F]FDG PET correctly diagnosed 40 of 46 malignant lesions (sensitivity = 87.0%). Once the PVE correction was considered in lesions smaller than 2.8 cm, the sensitivity of [^{18}F]FDG-PET diagnosis increased up to 97.8%, with 45 true-positive cases (using a cutoff value of 2.5 for pSUV).

In the present study, [^{18}F]FDG PET demonstrated low specificity in the differentiation between malignant and

Table 2. Patient Characteristics and Results of Immunohistochemistry (Nonmalignant Lesions).

Diagnosis	Size (mm)	SUV	pSUV	Indexes			Grade of Inflam	Comments
				P	*G*	*H*		
Tuberculosis	12	1.5	2.4	0	1	2	1	Necrosis (+)
Tuberculosis	15	4.1	6.9	0	2	3	1	Multiple granulomas
Tuberculosis	30	6.2	6.2	0	0	2	2	Necrosis (+), PCNA (+) in epithelial cells
Tuberculosis	30	22.4	22.4	0	2	1	3	Organizing pneumonia
Tuberculosis	43	4.5	4.5	0	3	1	1	Necrosis (+), fibrosis (+)
Tuberculosis	33	12.2	12.2	0	2	0	2	PCNA (+) in epithelial cells
Tuberculosis	25	3.2	3.3	0	1	2	1	Necrosis (+), calcification (+), fibrosis (+)
Tuberculosis	20	4.1	5	0	2	1	2*	Necrosis (+), calcification (+), fibrosis (+), chronic inflammation pattern
Tuberculosis	10	1.8	4.6	0	1	2	1	
Tuberculosis	10	5.7	20.1	0	1	2	3	Intra–air space granulomatous (+)
Total (TB)	22.8 ± 11.2	6.6 ± 6.3	8.8 ± 7.1	0	1.5 ± 0.8	1.6 ± 0.8	1.7 ± 0.9	
Chronic inflammation	18	2.4	3.3	0	0	0	3*	Chronic inflammation pattern, fibrosis (+), PCNA (+) in germinal center hyperplasia
Organizing pneumonia	20	5.2	6.5	0	0	0	3*	Chronic inflammation pattern, UIP pattern, fibrosis and smooth muscle cell proliferation (+), HK-II (+) in smooth muscle cell
Pulmonary sequestration	10	3.3	10.7	0	0	0	3	Pneumonia and bronchiolitis, chronic inflammation; smooth muscle cell proliferation (+); germinal center hyperplasia, HK-II (+) in smooth muscle cell
Paucilocalized fibrosis	10	1.7	3.3	0	0	0	1	Smooth muscle cell proliferation (+), fibrosis (+)
Total (non-TB)	14.5 ± 5.3	3.2 ± 1.5	6.0 ± 3.5	0	0	0	2.0 ± 1.4	
Total	20.4 ± 10.4	5.6 ± 5.5	8.0 ± 6.3	0	1.1 ± 1.0	1.1 ± 1.0	1.9 ± 0.8	

SUV = nonpartial volume effect corrected maxSUV; pSUV = partial volume effect corrected maxSUV; Grade of Inflam = grade of inflammatory process in the specimen; UIP = usual interstitial pneumonia; *P* = *P*-index; *G* = *G*-index; *H* = *H*-index; total (TB) = averaged values from pulmonary tuberculosis; total (non-TB) = averaged values from nonpulmonary tuberculosis.

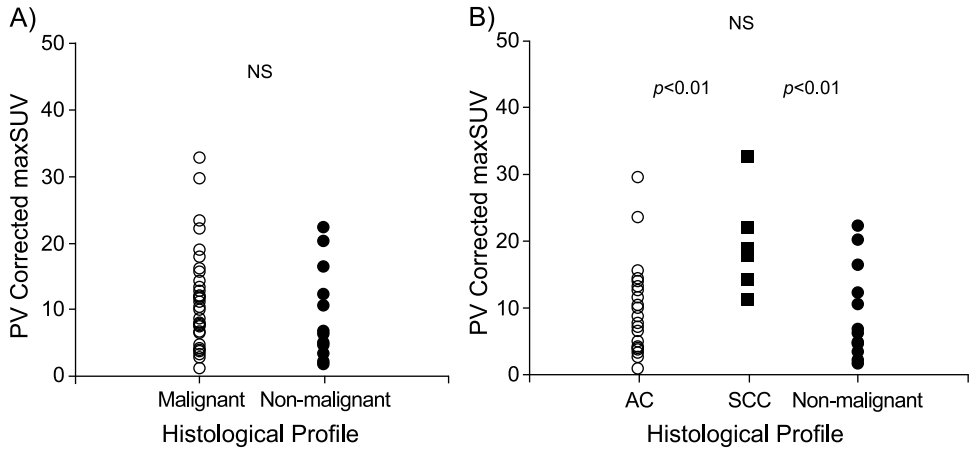

Figure 1. *pSUV values plotted with respect to tumor histologic diagnosis. (A) The pSUVs were higher for malignant lesions (mean ± SD, 10.9 ± 7.3) than that for nonmalignant lesions (8.0 ± 6.3) (NS). (B) The SCC showed the highest pSUV (mean ± SD, 19.5 ± 7.50) (ANOVA, P < 0.01). The AC lesions had higher pSUVs than that for nonmalignant lesions (NS). AC, adenocarcinoma of the lung; SCC, squamous cell carcinoma of the lung.*

nonmalignant lesions. Without PVE correction, the specificity was 21.4% with 11 false-positive cases, whereas specificity was 14.3% with 13 false-positive cases by the use of PVE correction. Therefore, the accuracy showed similar results in diagnoses using SUV and pSUV (76.7% and 78.3%, respectively).

Table 3. Results of Immunohistochemistry and Diagnostic Imaging (Malignant and Nonmalignant Lesions).

Histologic Features	Immunohistochemistry (+)			[^{18}F]FDG-PET (+) (pSUV > 2.5)
	PCNA	Glut-1	HK-II	
Malignant lesions				
Primary lesions				
Adenocarcinoma				
Well-differentiated (n = 14)	7/14	0/14	8/14	13/14
Moderately differentiated (n = 13)	8/13	7/13	11/13	13/13
Poorly differentiated (n = 5)	4/5	4/5	5/5	5/5
Total (n = 32)	19/32	11/32	24/32	31/32
SCC				
Well-differentiated (n = 1)	1/1	1/1	1/1	1/1
Moderately differentiated (n = 5)	5/5	5/5	5/5	5/5
Total (n = 6)	6/6	6/6	6/6	6/6
Neuroendocrine (large cell)	0/1	0/1	0/1	
Thymoma (lymphocyte-B1 type)	1/1	0/1	1/1	1/1
Pleomorphic carc (poorly differentiated)	1/1	1/1	0/1	1/1
				1/1
Metastatic lesions				
SCC	1/1	1/1	1/1	1/1
Adenocarcinoma	1/1	1/1	1/1	1/1
Renal cell carcinoma	1/1	1/1	1/1	1/1
Esophageal cancer	0/1	0/1	0/1	1/1
PNET	1/1	0/1	1/1	1/1
Total	31/46	21/46	34/46	45/46
Nonmalignant lesions				
Tuberculosis	0/10	9/10	9/10	9/10
Nontuberculosis	0/4	0/4	0/4	4/4
Total	0/14	9/14	9/14	13/14

Immunohistochemistry (+) = positive cases of PCNA, Glut-I, and HK-II expressions (grades 1–5); [^{18}F]FDG-PET (+) (pSUV > 2.5) = positive cases of [^{18}F]FDG-PET (+) by using a cutoff of 2.5; Percentage = percentage mean value of PCNA, Glut-1, and HK-II expressions; PNET = primary neuroendocrine tumor.

The pSUVs were higher for malignant lesions (10.9 ± 7.3) than those for nonmalignant lesions (8.0 ± 6.3), although this difference was not significant (Figure 1*A*). Among all pulmonary nodules evaluated in this study, the SCC showed the highest pSUV (19.5 ± 7.5) (ANOVA, $P < .01$). The pSUVs for AC (9.0 ± 6.3) were higher than that for nonmalignant lesions; however, this difference was not statistically significant (Figure 1*B*). pSUV did not show any correlation with stages of disease and sizes of tumor.

Immunohistochemical Findings

Tables 2–4 summarize the findings of the immunohistochemical analyses using anti–Glut-1, anti–HK-II, and anti-PCNA antibodies (*G*-index, *H*-index, and *P*-index, respectively). The scores for each index varied between three observers; however, the interobserver and intraobserver variabilities were less than one point in each case and were considered negligible in this study.

Primary non small cell lung cancer (NSCLC) Immunoreactivity of Glut-1 was mainly observed in the membrane of cancer cells; however, Glut-1 granules were also present in the cell cytoplasm (Figure 2, *A* and *B*). Positive cytoplasmic granules were observed more frequently in ACs than in SCCs. The expression of Glut-1 was often observed in cancer cells around necrotic sites (data not shown). No staining was observed in the section of negative controls (data not shown).

All SCC tissues were Glut-1–positive (Table 3). The average intensity of staining was significantly higher in SCCs (4.5 ± 0.7) than that for ACs (0.9 ± 1.4) ($P < .001$). As for ACs, the average intensity of Glut-1 staining was variable according to tumor differentiation (Table 4). However, all cases of well-differentiated AC were negative for Glut-1. The Glut-1 expression showed a close positive relationship with pSUV ($r = 0.66$, $P < .001$; Figure 3*A*) for malignant lesions.

A very fine uniform granular pattern was observed in the cytoplasm of most HK-II–positive cancer cells (Figure 2*D*). A similar result has been previously described by Brown et al. [33]. Smooth muscle cells and some macrophages in the airway showed HK-II–positive staining (Figure 4). All SCC tissues studied were HK-II–positive, as well as the poorly differentiated ACs (Table 3). The expression of HK-II in SCCs was higher (2.4 ± 1.7) than that for ACs (1.8 ± 1.5) (Table 4); however, this finding was not statistically significant. The HK-II expression showed a positive relationship with pSUV ($r = 0.43$, $P < .01$; Figure 3*B*). In well-differentiated ACs, all of them were negative for Glut-1, whereas 57.1% was positive for HK-II.

The PCNA expression was positive in all SCCs (Table 3) with a high intensity of PCNA-positive nuclei (2.6 ± 1.4) (Table 4). The number of PCNA-positive nuclei in ACs (1.3 ± 1.3) showed a smaller average value with wide deviation, compared to that in SCCs (NS). Table 3 summarizes the immunohistochemical findings for PCNA in malignant lesions. The *P*-index showed a significant correlation with pSUV ($r = 0.42$, $P < .01$; Figure 3*C*). In addition, the PCNA expression showed a closed positive correlation with Glut-1 or HK-II expression ($r = 0.58$, $P < .01$ and $r = 0.52$, $P < .01$; respectively) (Figure 5, *A* and *B*).

Concerning tumor differentiation of ACs (well, moderately, and poorly differentiated types), the poorly differentiated type showed the highest values of pSUV and *G*-index (ANOVA, $P < .05$ and $P < .001$, respectively). A linear regression analysis showed a significant correlation between *G*-index and tumor differentiation ($r^2 = 0.45$, $P < .001$; Figure 6). A significant relationship was also observed between *H*-index or pSUV and tumor differentiation ($r^2 = 0.14$, $P < .05$ and $r^2 = 0.26$, $P < .01$, respectively).

In some cases of primary NSCLC lesions, the inflammatory process was recognized both in the inside of the tumor tissues and in the surrounding interstitial spaces. The intensity was variable between specimens (0.8 ± 1.0) (Table 4), and no significant correlation was observed with *G*-index, *H*-index, or pSUV.

Other malignant lesions. The neuroendocrine tumor showed negative staining for all antibodies applied, whereas the thymoma and undifferentiated tumor had variable weak positive staining for Glut-1 or HK-II (Tables 3 and 4). Two of five metastatic lesions in the lung (SCC and AC) were diagnosed as pulmonary metastatic lesions from the primary site in the lung. The metastatic SCC had a high expression of all antibodies. Unexpectedly, the metastatic AC (well-differentiated type) showed a positive staining for anti–Glut-1 and HK-II. The other three nonpulmonary metastatic lesions showed variable staining (Tables 3 and 4).

Nonmalignant lesions. In TB, the Glut-1–positive staining was often localized in the membranes of granulocytes and macrophages around the necrotizing granulomas, as well as in the cytoplasm (Figure 2*C*). For the HK-II–positive staining, a uniform granular pattern of staining was also observed in the cytoplasm of granulocytes and macrophages in a similar manner described for Glut-1 (Figure 2*F*).

The Glut-1–positive staining was observed in 9 of 10 cases of TB (1.5 ± 0.8), whereas all non-TB lesions were Glut-1–negative stainings (Table 2). The HK-II–positive staining was also observed in 9 of 10 cases of TB (1.6 ± 0.8), with negative staining in non-TB lesions as well (Table 2). The *G*-index and *H*-index in nonmalignant lesions were smaller compared to that in malignant lesions (NS). The *G*-index and *H*-index did not show any significant correlation with pSUV for nonmalignant lesions. No staining was observed for PCNA antibody in all nonmalignant tissues.

In all cases of nonmalignant lesions, the inflammatory process was well recognized (Table 2). A chronic inflammatory process was observed in 2 of 10 patients with TB,

Table 4. Results of Immunohistochemistry (Malignant Lesions).

Diagnosis	Differentiation	Indexes			Grade of Inflam	Percentage (%)		
		P	*G*	*H*		PCNA	Glut-1	HK-II
Primary ($n = 41$)								
Adenocarcinoma ($n = 32$)	Well-differentiated ($n = 14$)	1.1 ± 1.4	0	1.4 ± 1.7	0.6 ± 0.9	18.4 ± 26.1	0	26.6 ± 33.4
	Moderately differentiated ($n = 13$)	1.4 ± 1.4	1.0 ± 1.2	1.8 ± 1.3	0.7 ± 0.9	25.0 ± 27.0	17.8 ± 23.3	32.2 ± 25.2
	Poorly differentiated ($n = 5$)	2.0 ± 1.4	2.8 ± 1.9	3.0 ± 1.6	1.6 ± 1.1	38.6 ± 25.9	54.6 ± 37.5	58.6 ± 30.7
	Total	1.3 ± 1.3	0.9 ± 1.4	1.8 ± 1.5	0.8 ± 1.0	24.3 ± 26.5	15.8 ± 27.4	34.0 ± 31.0
SCC ($n = 6$)	Well-differentiated ($n = 1$)	3	4	5	3	60	80	100
	Moderately differentiated ($n = 5$)	2.4 ± 1.7	4.4 ± 0.9	2.2 ± 1.9	1.0 ± 1.4	48.0 ± 33.5	88.0 ± 17.9	41.2 ± 38.1
	Total	2.6 ± 1.4	4.5 ± 0.7	2.4 ± 1.7	0.8 ± 1.3	48.8 ± 30.0	88.9 ± 16.1	46.7 ± 36.5
Neuroendocrine	–	0	0	0	0	0	0	0
Thymoma	–	2	0	1	3	33	0	20
Pleomorphic carc	Poorly differentiated	1	2	0	1	20	33	0
Metastatic ($n = 5$)								
Adenocarcinoma	Well-differentiated	4	2	5	0	73	40	100
SCC	Moderately differentiated	5	3	4	0	100	60	73
Renal Ca	Poorly differentiated	2	1	5	1	40	20	100
Esophageal Ca	Well-differentiated	0	0	0	1	0	0	0
PNET	–	1	0	1	0	20	0	13
Total ($n = 46$)		1.6 ± 1.5	1.3 ± 1.8	1.9 ± 1.7	0.8 ± 1.0	29.5 ± 29.2	25.9 ± 35.2	36.3 ± 33.8

Grade of Inflam = grade of inflammatory process in the specimen; Percentage = average percentage of anti-PCNA, anti–Glut-1, anti–HK-II antibody expression; *P* = *P*-index; *G* = *G*-index; *H* = *H*-index; SCC = squamous cell carcinoma; Ca = cancer; PNET = primary neuroendocrine tumor.

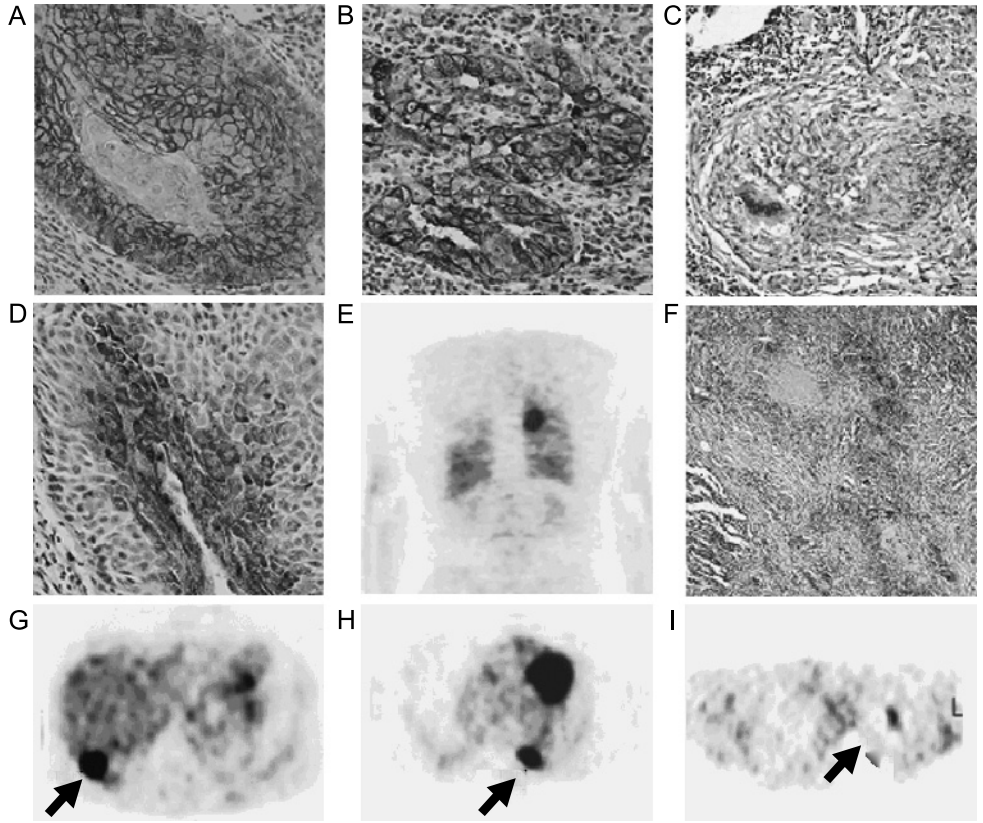

Figure 2. *Immunohistochemical findings and [^{18}F]FDG-PET examinations from selected patients enrolled in the present study. (A, D, and G) Glut-1 expression, HK-II expression, and [^{18}F]FDG-PET examination from the same patient (patient 33) with well-differentiated SCC, respectively. The highest expression of Glut-1 was observed in the membranes of cancer cells (grade 5) (original magnification, ×10), whereas the expression of HK-II was observed throughout the cytoplasm as small punctuate areas (grade 4) (original magnification, ×10). The [^{18}F]FDG-PET examination showed a high [^{18}F]FDG uptake in the posterior lower lobe of the right lung (panel G; arrow) on the transaxial slice (pSUV = 14.1). (B, E, and H) Glut-1 expression and two representative [^{18}F]FDG-PET reconstructed slices (coronal and transaxial slices, respectively) from a patient (patient 21) with AC (papillary type, moderate differentiated), respectively. The expression of Glut-1 can be observed in the membranes of cancer cells and as granules throughout the cell cytoplasm (grade 5) (original magnification, ×10). The [^{18}F]FDG PET examination showed a high uptake in the left lung (panel H; arrow) (pSUV = 12.4). (C, F, and I) Glut-1 expression, HK-II expression, and [^{18}F]FDG PET examination from a patient with pulmonary tuberculosis (patient 48), respectively. The expression of Glut-1 can be observed in the membranes of cells in the center of the pulmonary granuloma (grade 2) (original magnification, ×4), whereas the expression of HK-II can be observed in areas surround caseating granulomas throughout the cytoplasm (grade 3) (original magnification, ×4). The [^{18}F]FDG-PET examination showed a moderate [^{18}F]FDG uptake in the upper lobe of the left lung (panel I; arrow) on the transaxial slice (pSUV = 6.9).*

whereas a similar pattern was observed in half of the non-infectious specimens. The necrotic areas were frequently observed in tuberculosis patients, whereas fibrosis did not show any specific preferential lesion. The inflammatory process was significantly higher in nonmalignant lesions (1.93 ± 0.92) compared to malignant lesions (0.8 ± 1.0) ($P < .001$).

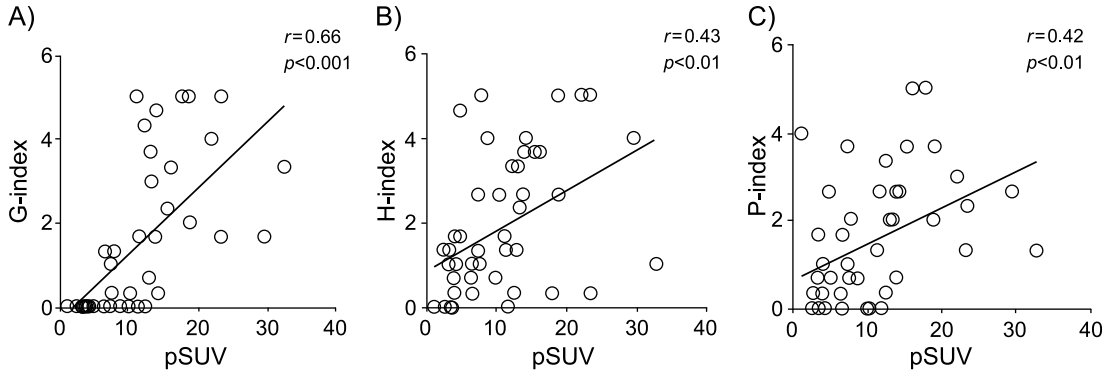

Figure 3. *Comparative analyses between grades of Glut-1 (G-index), HK-II (H-index), or PCNA (P-index) expressions with pSUV values in pulmonary malignant lesions. (A) The G-index showed a significant positive relationship with pSUV (r = 0.66, P < .001). (B) The H-index showed a significant positive relationship with pSUV (r = 0.43, P < .01). (C) The P-index showed a significant positive relationship with pSUV (r = 042, P < .01).*

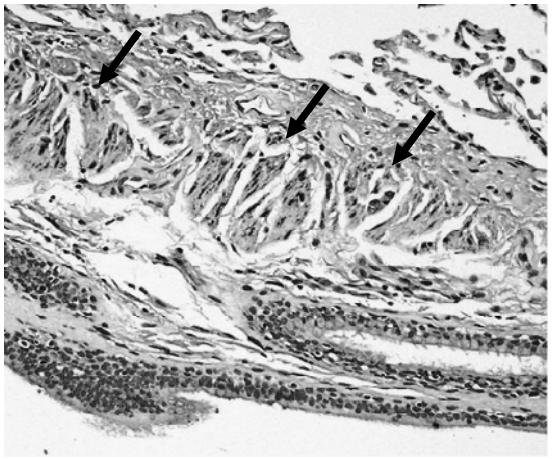

Figure 4. *Immunohistochemical findings from a selected patient (patient 20). In the present study, the HK-II expression in smooth muscle cells was often observed (arrow).*

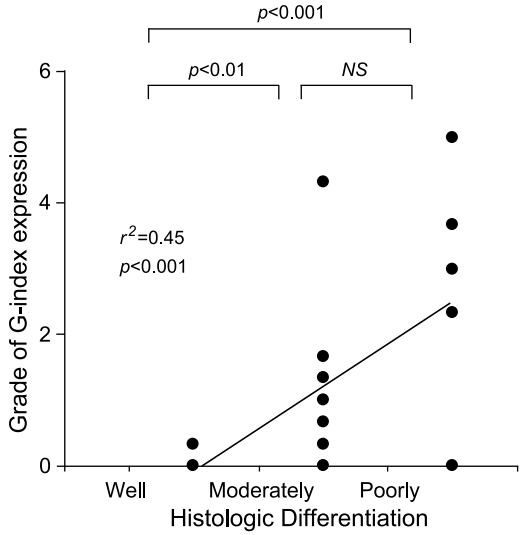

Figure 6. *Tumor histologic differentiations (well-moderated and poorly differentiated) plotted with respect to the grade of Glut-1 (G-index) expressions in AC of lung. The poorly differentiated AC of the lung showed the highest grade of anti–Glut-1 antibody expression (ANOVA, P < .001). No staining was observed in specimens from well-differentiated AC. A linear regression was observed between G-index and the grade of differentiation (r^2 = 0.45, P < .001).*

A close positive relationship was observed between the grading of inflammatory process and the pSUV (r = 0.61, P < .05; Figure 7) in nonmalignant lesions.

Discussion

[^{18}F]FDG-PET has been described as a useful method for differentiation between benign and malignant pulmonary lesions [15,19,20]. [^{18}F]FDG-PET has also been proved to be useful in the staging of known lung cancer [16,17]. In addition, [^{18}F]FDG-PET has become important in evaluating response to radiotherapy and/or chemoradiotherapy for NSCLC [21]. In a meta-analysis study evaluating 1474 focal pulmonary lesions of any size, Gould et al. [19] indicated that the sensitivity of [^{18}F]FDG-PET in detecting malignant lesions was between 83% and 100% (mean 96%), whereas specificity was extremely variable.

In the present study, the SUV values (non-PVE corrected) showed a high sensitivity of [^{18}F]FDG-PET to detect malignant lesions (87%), which is compatible with previous published data [15,19,20]. In order to increase the sensitivity of [^{18}F]FDG-PET in lung cancer, the correction of partial volume effect was carried out. The sensitivity increased up to 97.8%, once the partial volume effect was corrected (pSUV) using the RC for lesions smaller than 2.8 cm. This correction

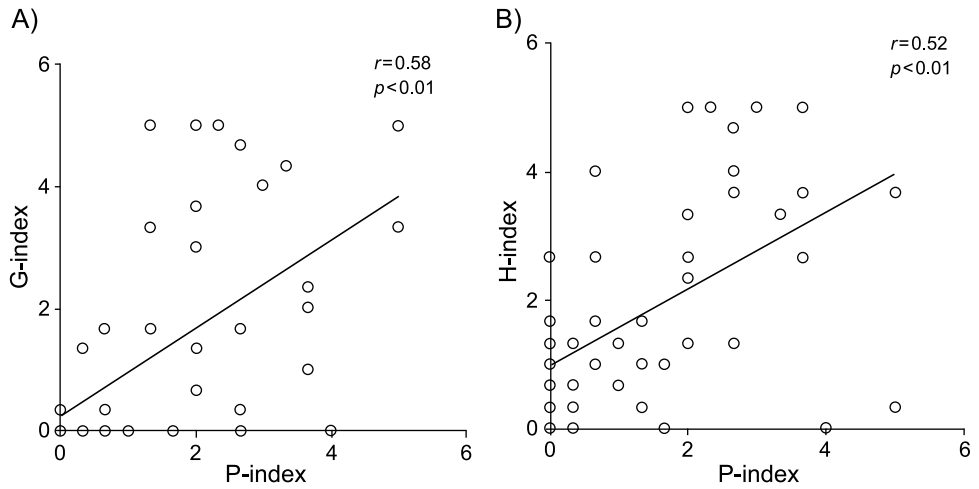

Figure 5. *A comparative analyses between grades of Glut-1 (G-index) or HK-II (H-index) expressions, with grade of PCNA (P-index) expressions in pulmonary malignant lesions. (A) The G-index and P-index showed a significant positive relationship (r = 0.58, P < .01). (B) The H-index and P-index showed a significant positive relationship (r = 0.52, P < .01).*

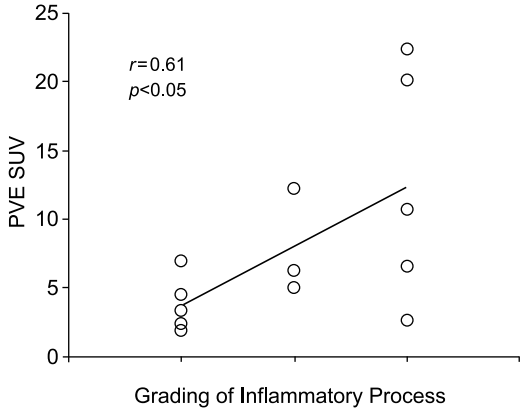

Figure 7. *A comparative analysis between pSUV values and grade of inflammatory process in nonmalignant lesions. A linear regression was observed between pSUV and the grade of inflammation ($r^2 = 0.61$, $P < .05$).*

appears to be a valuable tool to evaluate small pulmonary lesions. The PVE leads to underestimation when the structure is smaller than twice the full width at half-maximum scanner resolution [34]. Such partial volume effects are particularly of note when tissue characteristics derived from the analysis of microscopic specimens are compared to PET data. However, the specificity in our study (21.4% and 14.3%) was lower than those reported in previous studies for both analyses (SUV and pSUV, respectively) [15,19,20]. This fact could be attributed to a relatively high incidence of granulomas in our population and to the selection criteria of the population (all lesions were surgically resected).

In order to differentiate malignant and nonmalignant lesions, the uptake of [^{18}F]FDG, translated as SUV, is widely used in clinical practice. As expected, we observed higher pSUV values in pulmonary malignant lesions compared to nonmalignant lesions. The SCCs showed significantly higher pSUV values than those of nonmalignant lesions and ACs. However, ACs lesions did not show any significant difference compared to nonmalignant lesions. Therefore, the differential diagnosis between ACs and nonmalignant lesions may be difficult by use of quantitative analysis of [^{18}F]FDG-PET.

Three steps are required for [^{18}F]FDG accumulation in cancer cells: 1) facilitated diffusion through glucose transport proteins; 2) subsequent phosphorylation by hexokinase isoforms producing FDG-6-phosphate (FDG-6-P); and 3) decreased dephosphorylation. It is believed that the dephosphorylation process is negligible and the [^{18}F]FDG-6-P is neither transported out of cells nor subjected to glycolytic breakdown; it is metabolically trapped inside cells. Thus, [^{18}F]FDG accumulation depends basically on the rate of transport through the cell membrane and the activity of hexokinase [35,36].

Several subtypes of the human facilitative glucose transporters have been described [37]. Glut-1 is the main subtype that has been shown to overexpress in NSCLC [10–13], whereas the contribution of the other transporters to the overall glucose metabolism in NSCLC appears to be minor [13]. Although several hexokinase subtypes have also been described, Hexokinase II is suggested to be the main subtype in regulating glucose metabolism in cancer cells [14]. Therefore, in the present study, we examined solely the expression of Glut-1 and HK-II in lung nodules.

In our series, substantial differences in Glut-1 expression were found in primary lesions of NSCLC of different histology, in which a close correlation between Glut-1 expression and [^{18}F]FDG uptake was observed in NSCLC. These results suggest that the overexpression of Glut-1 may have an important role in the survival of cancer cells by promoting adequate energy supply in an often-less-than-ideal physiological environment [38,39]. The expression of Glut-1 in SCC was higher than in AC, which has also been found in previous studies [11,13]. Based on this higher transport activity in SCC, we assume that the [^{18}F]FDG uptake in SCCs is higher than that in AC lesions. The Glut-1 expression in NSCLC localized preferentially in the edge of the necrotic regions corresponding to the hypoperfused area. Previous studies have observed similar findings [11,13].

To our knowledge, this is the first immunohistochemical study that evaluates HK-II expression and FDG uptake in NSCLC. The HK-II expression in SCCs showed a higher level compared to that of ACs. In addition, the present study also showed a close correlation between the presence of HK-II and [^{18}F]FDG uptake of NSCLC. Several previous studies have suggested the possibility that Glut-1 plays a role of rate-limiting step in the uptake of [^{18}F]FDG in cancer cells including primary lung cancer cells [10,11,13]. From the present study, however, we may conclude that both Glut-1 and HK-II are important and closely related to each other.

The degree of cell differentiation correlates with either Glut-1 or HK-II expressions in AC of the lung. In terms of Glut-1 expression, a similar result has been reported by Ito et al. [11]. However, no studies related to HK-II and the degree of differentiation of AC in lung cancer have been published. In ACs of the well-differentiated type, both the low Glut-1 and HK-II expressions seem to be the reason for the low uptake of [^{18}F]FDG.

To estimate tumor aggressiveness and to determine patients' prognoses, the measurement of the proliferation rate of tumor cells in lung carcinoma is an essential feature. PCNA, also known as cyclin or auxiliary protein for DNA polymerase δ, is a 36-kDa nuclear polypeptide that is directly involved in DNA synthesis [40]. Immunohistochemical detection of PCNA has been extensively applied to investigate the proliferation rate of tumor cells in various types of malignancy [31,41]. In our study population, the [^{18}F]FDG uptake correlated with proliferative potential measured by PCNA in NSCLC. Concordant findings have been previously published [32,42]. We have also observed a good correlation between PCNA expression with either Glut-1 and HK-II expressions. In tumors with high proliferative potential, glucose metabolism may also increase to produce enough energy for proliferation.

[^{18}F]FDG is not a tumor-specific tracer. As a result of increased glycolytic activity, inflammatory cells such as neutrophils, activated macrophages, and lymphocytes also

have increased [^{18}F]FDG uptake, producing high [^{18}F]FDG accumulation at sites of inflammation and infection [22–25]. However, the mechanisms of uptake by these cells are still not completely understood.

The uptake of [^{18}F]FDG in the whole tumor is considered to be combined uptake in both neoplastic and non-neoplastic cellular components [43,44]. Our previous study, using an animal experimental model, indicates the importance of cellular immunity employed by T-lymphocytes for [^{18}F]FDG uptake in tumors [45]. Therefore, in our series, we had expected that the inflammatory process in the malignant lesions (expressed as a grade of inflammation) affects FDG uptake in whole tumor tissues. It seems, however, that the contribution of inflammatory process to the overall [^{18}F]FDG uptake in NSCLC is not substantial.

In the present study, we observed a substantial expression of Glut-1 and HK-II in TB. They were expressed at the edge of the granulomatous tissue, which has a high accumulation of macrophages. This finding explains the relatively high [^{18}F]FDG uptake in pulmonary TB. Concerning non-TB lesions, there was a lack of expression of Glut-1 and HK-II. A report suggested a possibility that some specific lesions are more likely to increase the [^{18}F]FDG uptake than others, depending on the type of inflammatory cells presented at the infectious/inflammatory sites [46]. However, we have no data to explain our present results so far. However, we observed a positive correlation between grading of inflammation and [^{18}F]FDG uptake in inflammatory lesions, which suggests that inflammatory cells can take in [^{18}F]FDG, not using solely the expression of Glut-1 or HK-II, but using the expression of some other glucose transporters or hexokinases, or others. Further examination is needed.

One of the limitations of the present study was the relative lack of precision in ROI positioning of pulmonary lesions with low FDG uptake. We used the corresponding CT images to give the best position, although misregistration may occur in such cases. Improvements would be made by the introduction of PET/computed tomography (CT) technology. PET/CT has been shown to be more accurate in characterizing pulmonary lesions, especially lymphadenopathy [47]. Utility of PET/CT may make it possible to have a similar comparative study between FDG uptake and immunoreactivity even in small lymph nodes in the mediastinum. Another weak point in the present study was the grading system of inflammation applied. A well-experienced pathologist in lung disease (M.K.) defined the inflammatory process based on clinical experience, and reviewed the specimen twice. There was no difference in the results between these two trials, which implied the stability of the grading. However, interobserver variances were not evaluated in the present study.

Despite the original promise of [^{18}F]FDG PET imaging for pulmonary disease—that it would allow noninvasive discrimination between benign and malignant lesions—we have noted that it was not completely fulfilled. With the future development of new compounds that are less influenced by inflammatory processes, there will be an increase in the specificity of PET studies [47]. Recently, Van Waarde et al. [23] suggested in their rodent model the possible usefulness of ^{18}F FLT in the differentiation between malignancies and benign lesions, compared to FDG. Further evaluation is needed in human specimens.

Conclusions

Our study indicates that the uptake of [^{18}F]FDG in lung cancer correlates well with Glut-1, HK-II, and PCNA expressions. As for nonmalignant pulmonary lesions, the presence of a higher inflammatory process correlated with the uptake of [^{18}F]FDG. These findings suggest that severe inflammatory process may affect [^{18}F]FDG uptake; therefore, differential diagnosis between malignant and nonmalignant lesions of the lungs should be performed carefully.

Acknowledgements

The authors would like to thank Toru Fujita for his valuable help during imaging acquisition, the technologists from the Department of Pathology for their incredible help in preparing the specimens, and Jorge A. Carrasquillo of the National Institutes of Health for his valuable suggestions and editorial contributions.

References

[1] Jemal A, Tiwari RC, Murray T, Ghafoor A, Samuels A, Ward E, Feuer EJ, and Thun MJ (2004). Cancer statistics, 2004. *CA Cancer J Clin* **54,** 8–29.

[2] Editorial Board of the Cancer Statistics in Japan (2003). In Foundation for Promotion on Cancer Research, (Ed.). Cancer Statistics in Japan 2003, 1–77 Foundation for Promotion of Cancer Research (FPCR), Tokyo.

[3] Warburg O, Posener K, and Negelein E (1931). The metabolism of the carcinoma cell. In Warburg, O (Ed.), The Mechanism of Tumors, pp. 129–169 Richard R. Smith, Inc., New York, NY.

[4] Weber G (1977). Enzymology of cancer cells. *N Engl J Med* **296,** 486–493.

[5] Merrall NW, Plevin R, and Gould GW (1993). Growth factors, mitogens, oncogenes and the regulation of glucose transport. *Cell Signal* **5,** 667–675.

[6] Birnbaum MJ, Haspel HC, and Rosen OM (1987). Transformation of rat fibroblasts by FSV rapidly increases glucose transporter gene transcription. *Science* **235,** 1495–1498.

[7] Parry DM and Pedersen PL (1983). Intracellular localization and properties of particulate hexokinase in the Novikoff ascites tumor. Evidence for an outer mitochondrial membrane location. *J Biol Chem* **258,** 10904–10912.

[8] Paul R, Johansson R, Kellokumpu-Lehtinen PL, Soderstrom KO, and Kangas L (1985). Tumor localization with ^{18}F-2-fluoro-2-deoxy-D-glucose: comparative autoradiography, glucose 6-phosphatase histochemistry, and histology of renally implanted sarcoma of the rat. *Res Exp Med* **185,** 87–94.

[9] Graham MM, Spence AM, Muzi M, and Abbott GL (1989). Deoxyglucose kinetics in a rat brain tumor. *J Cereb Blood Flow Metab* **9,** 315–322.

[10] Younes M, Lechago LV, Somoano JR, Mosharaf M, and Lechago J (1996). Wide expression of the human erythrocyte glucose transporter Glut1 in human cancers. *Cancer Res* **56,** 1164–1167.

[11] Ito T, Noguchi Y, Satoh S, Hayashi H, Inayama Y, and Kitamura H (1998). Expression of facilitative glucose transporter isoforms in lung carcinomas: its relation to histologic type, differentiation grade, and tumor stage. *Mod Pathol* **11,** 437–443.

[12] Kurata T, Oguri T, Isobe T, Ishioka S, and Yamakido M (1999). Differential expression of facilitative glucose transporter (GLUT) genes in primary lung cancers and their liver metastases. *Jpn J Cancer Res* **90,** 1238–1243.

[13] Brown RS, Leung JY, Kison PV, Zasadny KR, Flint A, and Wahl RL (1999). Glucose transporters and FDG uptake in untreated primary human non-small cell lung cancer. *J Nucl Med* **40,** 556–565.

[14] Mathupala SP, Rempel A, and Pedersen PL (1997). Aberrant glycolytic metabolism of cancer cells: a remarkable coordination of genetic, transcriptional, post-translational, and mutational events that lead to a critical role for type II hexokinase. *J Bioenerg Biomembr* **29,** 339–343.

[15] Patz EF Jr, Lowe VJ, Hoffman JM, Paine SS, Burrowes P, Coleman RE, and Goodman PC (1993). Focal pulmonary abnormalities: evaluation with F-18 fluorodeoxyglucose PET scanning. *Radiology* **188,** 487–490.

[16] Gupta NC, Graeber GM, Rogers JS, and Bishop HA (1999). Comparative efficacy of positron emission tomography with FDG and computed tomographic scanning in preoperative staging of non-small cell lung cancer. *Ann Surg* **229,** 286–291.

[17] Marom EM, McAdams HP, Erasmus JJ, Goodman PC, Culhane DK, Coleman RE, Herndon JE, and Patz EF Jr (1999). Staging non-small cell lung cancer with whole-body PET. *Radiology* **212,** 803–809.

[18] Munley MT, Marks LB, Scarfone C, Sibley GS, Patz EF Jr, Turkington TG, Jaszczak RJ, Gilland DR, Anscher MS, and Coleman RE (1999). Multimodality nuclear medicine imaging in three-dimensional radiation treatment planning for lung cancer: challenges and prospects. *Lung Cancer* **23,** 105–114.

[19] Gould MK, Maclean CC, Kuschner WG, Rydzak CE, and Owens DK (2001). Accuracy of positron emission tomography for diagnosis of pulmonary nodules and mass lesions: a meta-analysis. *JAMA* **285,** 914–924.

[20] Keith CJ, Miles KA, Griffiths MR, Wong D, Pitman AG, and Hicks RJ (2002). Solitary pulmonary nodules: accuracy and cost-effectiveness of sodium iodide FDG-PET using Australian data. *Eur J Nucl Med Mol Imaging* **29,** 1016–1023.

[21] Mac Manus MP, Hicks RJ, Matthews JP, McKenzie A, Rischin D, Salminen EK, and Ball DL (2003). Positron emission tomography is superior to computed tomography scanning for response-assessment after radical radiotherapy or chemoradiotherapy in patients with non-small-cell lung cancer. *J Clin Oncol* **21,** 1285–1292.

[22] Bakheet SM, Saleem M, Powe J, Al-Amro A, Larsson SG, and Mahassin Z (2000). F-18 fluorodeoxyglucose chest uptake in lung inflammation and infection. *Clin Nucl Med* **25,** 273–278.

[23] Van Waarde A, Cobben DCP, Suurmeijer AJH, Maas B, Vaalburg W, de Vries EFJ, Jager PL, Hoekstra HJ, and Elsinga PH (2004). Selectivity of ^{18}F-FLT and ^{18}F-FDG for differentiating tumor from inflammation in a rodent model. *J Nucl Med* **45,** 695–700.

[24] Goo JM, Im JG, Do KH, Yeo JS, Seo JB, Kim HY, and Chung JK (2000). Pulmonary tuberculoma evaluated by means of FDG PET: findings in 10 cases. *Radiology* **216,** 117–121.

[25] Croft DR, Trapp J, Kernstine K, Kirchner P, Mullan B, Galvin J, Peterson MW, Gross T, McLennan G, and Kern JA (2002). FDG-PET imaging and the diagnosis of non-small cell lung cancer in a region of high histoplasmosis prevalence. *Lung Cancer* **36,** 297–301.

[26] Hamacher K, Coenen HH, and Stocklin G (1986). Efficient stereospecific synthesis of no-carrier-added 2-[^{18}F]-fluoro-2-deoxy-D-glucose using aminopolyether supported nucleophilic substitution. *J Nucl Med* **27,** 235–238.

[27] Kitano H, Magata Y, Tanaka A, Mukai T, Kuge Y, Nagatsu K, Konishi J, and Saji H (2001). Performance assessment of O-18 water purifier. *Ann Nucl Med* **15,** 75–78.

[28] Akashi Y, Kuwabara Y, Ichiya Y, Sasaki M, Yoshida T, Fukumura T, and Masuda K (1994). The partial volume effect correction for pulmonary mass lesions using a ^{68}Ga/^{68}Ge transmission scan in PET study. *Kaku Igaku* **31,** 1511–1517.

[29] Vessele H, Schmidt RA, Pugsley JM, Li M, Kohlmyer SG, Vallieres E, and Wood DE (2000). Lung cancer proliferation correlates with ^{18}F-fluorodeoxyglucose uptake by Positron Emission Tomography. *Clin Cancer Res* **10,** 3837–3844.

[30] Miyauchi T and Wahl RL (1996). Regional 2-[^{18}F]fluoro-2-deoxy-D-glucose uptake varies in normal lung. *Eur J Nucl Med* **23,** 517–523.

[31] Higashi T, Saga T, Nakamoto Y, Ishimori T, Mamede MH, Wada M, Doi R, Hosotani R, Imamura M, and Konishi J (2002). Relationship between retention index in dual-phase ^{18}F-FDG PET, and hexokinase-II and glucose transporter-1 expression in pancreatic cancer. *J Nucl Med* **43,** 173–180.

[32] Higashi K, Ueda Y, Yagishita M, Arisaka Y, Sakurai A, Oguchi M, Seki H, Nambu Y, Tonami H, and Yamamoto I (2000). FDG PET measurement of the proliferative potential of non-small cell lung cancer. *J Nucl Med* **41,** 85–92.

[33] Brown RS, Goodman TM, Zasadny KR, Greenson JK, and Wahl RL (2002). Expression of hexokinase II and Glut-1 in untreated human breast cancer. *Nucl Med Biol* **29,** 443–453.

[34] Keyes JW Jr (1995). SUV: standard uptake or silly useless value? *J Nucl Med* **36,** 1836–1839.

[35] Haberkorn U, Ziegler SI, Oberdorfer F, Trojan H, Haag D, Peschke P, Berger MR, Altmann A, and van Kaick G (1994). FDG uptake, tumor proliferation and expression of glycolysis associated genes in animal tumor models. *Nucl Med Biol* **21,** 827–834.

[36] Golshani-Hebroni SG and Bessman SP (1997). Hexokinase binding to mitochondria: a basis for proliferative energy metabolism. *J Bioenerg Biomembr* **29,** 331–338.

[37] Mueckler M (1994). Facilitative glucose transporters. *Eur J Biochem* **219,** 713–725.

[38] Sebastian S and Kenkare UW (1997). Insulin-like growth factor I induces tumor hexokinase RNA expression in cancer cells. *Biochem Biophys Res Commun* **235,** 389–393.

[39] Newsholme EA and Board M (1991). Application of metabolic-control logic to fuel utilization and its significance in tumor cells. *Adv Enzyme Regul* **31,** 225–246.

[40] Mathews MB, Bernstein RM, Franza BR Jr, and Garrels JI (1984). Identity of the proliferating cell nuclear antigen and cyclin. *Nature* **309,** 374–376.

[41] Brown RS, Leung JY, Fisher SJ, Frey KA, Ethier SP, and Wahl RL (1995). Intratumoral distribution of tritiated fluorodeoxyglucose in breast carcinoma: I. Are inflammatory cells important? *J Nucl Med* **36,** 1854–1861.

[42] Duhaylongsod FG, Lowe VJ, Patz EF Jr, Vaughn AL, Coleman RE, and Wolfe WG (1995). Lung tumor growth correlates with glucose metabolism measured by FDG PET. *Ann Thorac Surg* **60,** 1348–1352.

[43] Steele RJ, Brown M, and Eremin O (1985). Characterisation of macrophages infiltrating human mammary carcinomas. *Br J Cancer* **51,** 135–138.

[44] Kubota K, Kubota R, and Yamada S (1993). FDG accumulation in tumor tissue. *J Nucl Med* **34,** 419–421.

[45] Mamede M, Saga T, Ishimori T, Nakamoto Y, Sato N, Higashi T, Mukai T, Kobayashi H, and Konishi J (2003). Differential uptake of ^{18}F-fluorodeoxyglucose by experimental tumors xenografted into immunocompetent and immunodeficient mice and the effect of immunomodification. *Neoplasia* **5,** 179–183.

[46] Zhuang HM, Lee JH, Pourdehnad M, Atochina O, Rossman MD, and Alavi A (1999). *In vitro* investigation of FDG uptake in human inflammatory cells[Abstract] . *J Nucl Med* **40,** 198.

[47] Cerfolio RJ, Ojha B, Bryant AS, Raghuveer V, Mountz JM, and Bartolucci A (2004). The accuracy of integrated PET-CT compared with dedicated PET alone for the staging of patients with nonsmall cell lung cancer. *Ann Thorac Surg* **78,** 1017–10123.